Article:
Mohan, Ashutosh, Chaurasia, S., Rao, Usha et al. (1 more author) (2021) Time-Resolved Raman Spectroscopy of Hexafluorobenzene (C6F6) under Laser-Driven Shock Compression. Journal of Quantitative Spectroscopy and Radiative Transfer. 107547. ISSN 0022-4073

https://doi.org/10.1016/j.jqsrt.2021.107547

Time-Resolved Raman Spectroscopy of Hexafluorobenzene (C_6F_6) under Laser-Driven Shock Compression

Ashutosh Mohan , S. Chaurasia , Usha Rao , John Pasley

PII: S0022-4073(21)00040-6
DOI: https://doi.org/10.1016/j.jqsrt.2021.107547
Reference: JQSRT 107547

To appear in: *Journal of Quantitative Spectroscopy & Radiative Transfer*

Received date: 19 November 2020
Revised date: 25 January 2021
Accepted date: 27 January 2021

Please cite this article as: Ashutosh Mohan , S. Chaurasia , Usha Rao , John Pasley , Time-Resolved Raman Spectroscopy of Hexafluorobenzene (C_6F_6) under Laser-Driven Shock Compression, *Journal of Quantitative Spectroscopy & Radiative Transfer* (2021), doi: https://doi.org/10.1016/j.jqsrt.2021.107547

Time-Resolved Raman Spectroscopy of Hexafluorobenzene (C_6F_6) under Laser-Driven Shock Compression

Ashutosh Mohan[1], S. Chaurasia*[1, 2], Usha Rao[1, 3], John Pasley[4]

[1] *High Pressure and Synchrotron Radiation Physics Division, Bhabha Atomic Research Centre, Mumbai-400085, India*

[2]*HomiBhabha National Institute, Mumbai-400094, India*

[3]*University of Mumbai, Mumbai-400032, India*

[4]*York Plasma Institute, Department of Physics, University of York, York, YO10 5DQ, UK*

***shibu@barc.gov.in**

Highlights

- Time resolved Raman Spectroscopy of the hexafluorobenzene under extreme conditions at molecular level has been done.
- The phase transitions under high pressure has been studies
- One Dimensional hydrodynamic simulation is performed to validate the experimental data.
- Laser driven flyer is developed for the shock compression in the hexafluorobenzene sample

Abstract:

Hexafluorobenzene is used as a cooling fluid in nuclear reactors, production of pharmaceutical compounds and in prognostic biomarkers. It is useful to understand the dynamics of Hexafluorobenzene under extreme conditions. For the first time, we have performed Time-resolved Raman Spectroscopy of laser shocked Hexafluorobenzene using a pump-probe technique to study the effect of high pressure at the molecular level and possible phase transitions. A 2 J / 8 ns Nd: YAG laser system is used for generating shock pressures of up to 4.5 GPa in the sample in a confined geometry. Three prominent modes at 370 cm^{-1} (e_{1g} fundamental mode or ν_{10}), 445 cm^{-1} (e_{2g} fundamental mode or ν_6) and 560 cm^{-1} (a_{1g} fundamental mode or ν_1) exhibit blue shift with scaling factors of 370 + 0.88 P(GPa), 445 +1.22P(GPa) and 560 +1.93P(GPa) respectively. A liquid→Phase-II phase transition is observed at a pressure of 0.9 GPa which is very close to the 0.8 GPa pressure at which a phase transition has been reported to occur under static compression. The shock velocity in Hexafluorobenzene at a laser energy of 300 mJ and 500 mJ is calculated by measuring the intensity ratio of Raman modes emerging from the shocked region to that of the whole

sample. To validate the experimental results, 1-D radiation hydrodynamics simulations are also performed. Experimentally obtained shock velocities, at a laser intensity of 1.47 GW/cm ^{2} (300 mJ) and 2.46 GW/cm^2 (500 mJ), are 2.54 km/s and 3.65 km/s respectively which are in close agreement with simulation results of 2.98 km/s and 3.84 km/s respectively. Gruneisen parameters corresponding to the three modes are also calculated which are 0.00950 ± 0.0140 (ν_{10} mode), 0.0433 ± 0.0060 (ν_6 mode), and 0.0561 ± 0.0044 (ν_1 mode) respectively.

Keywords: Laser-driven shock wave, Time-resolved Raman Spectroscopy, Phase transition, molecular spectroscopy

Introduction:

For years, high-pressure studies have been of importance to several other research areas such as astrophysical research [1], geological and planetary studies [2], inertial confinement fusion (ICF) research [3] and condensed matter physics [4] to name a few. Shock wave experiments are a reliable means of providing information about the dynamics of thermo-physical, chemical, and mechanical properties of matter under extreme conditions (high-pressure and high-temperature). Conventional shock wave experiments, using streak cameras and interferometers, provide end-state information only. However, real-time information is of the utmost importance in understanding the phenomena induced by a shock wave propagating through a material [5] which can be achieved only by time-resolved x-ray or optical spectroscopy measurements. Vibrational spectroscopy, a branch of optical spectroscopy, is a suitable tool to probe such phenomena as it allows the monitoring of molecular, structural, and chemical changes directly [6].

The development of high-intensity lasers has provided a reliable alternative to the shock wave experiments usually performed using gas guns, impact loading [7], energetic materials [8], and historically in underground nuclear tests [9]. Such high-intensity laser driven shock wave experiments have several potential advantages such as high repeatability and stability, low cost, compactness and high achievable peak pressures [10, 11]. Apart from this, the generation of short pulses of the order of femtoseconds to nanoseconds from lasers is also useful for real-time understanding of chemical processes as most of the chemical reaction dynamics transpire in the time frame of 10^{-13} to 10^{-9} seconds. In laser-driven shock wave experiments, a high-intensity laser pulse is focused onto the target, thereby generating rapidly expanding plasma which in turn launches a shock wave into the target and hence

dynamically compresses it. To understand shock-induced phenomena occurring on nanosecond time-scales, it is necessary to probe at a similar time-scales. Time-resolved Raman spectroscopy (TRRS) is a very capable and efficient tool for the investigation of molecular and chemical changes triggered by dynamic pressure on nanosecond timescales as it provides real-time information about the changes occurring in the sample due to the propagation of the shock wave [12]. Hence, of late, laser-based TRRS has been garnering significant attention.

Over the past few decades, fluorination has emerged as an effective way of achieving useful properties in materials that find use in various aspects of science as well as everyday life. Fluorinated compounds, because of the strength of the C-F bond, exhibit weak intermolecular interactions, high oxidative and thermal stability, low polarity, and surface tension in comparison to their hydrocarbon counterparts. These properties have led to the development of various new materials such as liquid crystals, conductive polymers, dyes, pharmaceuticals, etc. [13-17]. Fluorocarbons are also a potential source of molecular fluorine [18]. Hexafluorobenzene (C_6F_6) is a derivative of benzene obtained by H/F atoms substitution. It is widely used as a solvent in various NMR spectroscopy and photochemical reactions. Its properties allow it to be used in the production of dyes, pigments, explosives, and fungicides and also in air conditioning systems as an algaecide in coolant water [19]. Hexafluorobenzene has extremely widespread use in the biomedical field (cancer research) as it is used in investigating potential prognostic biomarkers of tumour oxygenation because of its single and narrow NMR signal and high sensitivity [20, 21]. Hexafluorobenzene (C_6F_6) has many properties similar to that of benzene (C_6H_6) such as freezing point (~ 278 K) and boiling point (~ 353.5 K) and they both exhibit one solid phase upon cooling [22-25]. Both have been shown to exhibit high-pressure phases too [25-27]. There are several studies available on static compression of Benzene [28, 29], Hexafluorobenzene [18, 30] as well as C_6H_6-C_6F_6 co-crystal [31]. Suzuki et al. demonstrated that when C_6F_6 is compressed slowly at room temperature, beyond 0.3 GPa, a dendrite phenomenon was observed and it solidifies into phase-I at about 1 GPa and then into phase-II on further compression (2-4 GPa); on the other hand, on the quick application of pressure up to 0.8 GPa, it solidifies directly into phase-II [18]. In this experiment, it was observed that Phase-I does not reverse back to the liquid state when the pressure is released; however, phase-II returns to the original liquid state and thereby undergoes a reversible phase transition. M. Pravica et al. extended this study further up to 34.4 GPa and reported up to 5 different phases using Raman, IR, and

angular dispersive XRD techniques [30]. When compressed using laser-driven shock waves, materials experience a sudden and extreme compression along with significantly high temperatures.

In this manuscript, we present phase transitions observed in Hexafluorobenzene under laser-driven shock compression by using the pump-probe technique and its comparison with published static compression data. We also performed time-resolved spectroscopy of the sample to study the shock wave propagation through the sample which enables us to determine the shock velocity using experimental data. To validate the experimental data, we also performed a 1-D radiation-hydrodynamics simulation and the results are in good agreement with the experimental data.

Experimental Details:

The experiments are performed using a Q-switched high-power neodymium-doped yttrium aluminium garnet (Nd: YAG) pulsed laser (2 J / 8 ns EKSPLA Laser) in a pump-probe configuration. A fundamental beam (1064 nm / 8 ns) of the laser is used as a pump for launching the shock wave into the sample and a second harmonic beam (532 nm / 8 ns) is used as a probe for exciting Raman scattering in the sample. The spatial profile of the laser is nearly flat (80% hat top profile) which ensures uniform shock pressure in and around the region being probed. To probe the sample at different time intervals, the optical delay between pump and probe is generated by using two large-size plane mirrors arranged in parallel geometry with a gap of 1.05 meters (roundtrip time 7 ns). The sample is prepared in a confined geometry with the target assembly consisting of a 2.5 mm thick cover glass (20 mm diameter) with 25 µm thick aluminium foil glued to it, followed by a 200 µm thick Teflon spacer, and a further layer of glass (same as the cover glass). In this confined geometry, the sample occupies the volume created by the spacer between the two glass plates. Such a target assembly helps to enhance the shock pressure by 6 times and increases the shock pressure pulse profile duration by a factor of 10 [32]. The schematic of the experimental setup has been shown in figure 1. More details about it can be found in earlier works [33, 34].

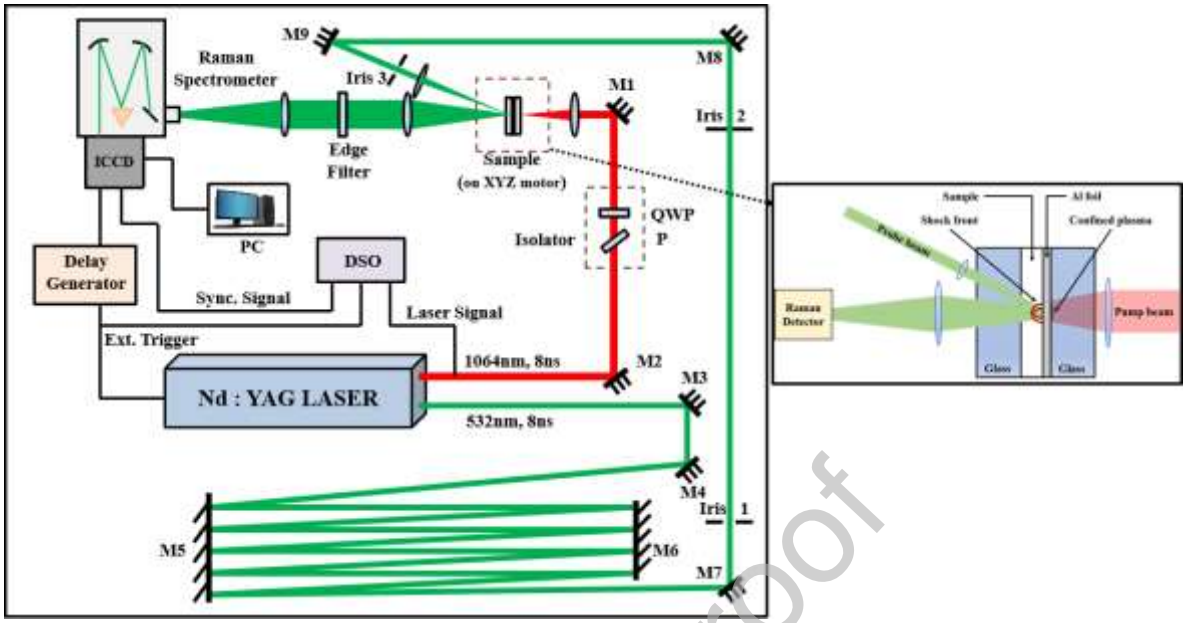

Fig. 1. Schematic of the experimental setup; $M_{1\text{-}9}$ are reflecting mirrors, P is a polarizer, QWP is a quarter-wave plate, DSO is digital scope & ICCD is an intensified charge-coupled device [33].

The pump beam is focused on the target assembly at the glass-aluminium interface, within a spot size of 1.8 mm diameter, which generates plasma at the interface. This plasma plume expands backward and is confined by the cover glass (hence it is referred to as a confined geometry) which results in an enhanced amplitude shock wave being driven into the aluminium foil. A stable shock wave generated in the aluminium foil which then enters into the sample at the aluminium-sample interface. The magnitude of shock pressure reduces in the sample due to the lower shock impedance of C_6F_6; for example, with a 500 mJ laser pulse, the shock pressure in aluminium is 5.7 GPa which drops down to 2.6 GPa upon entering the sample. Coincident with the passage of this shock wave, the sample gets dynamically compressed. From the rear side, the probe beam is focused onto the centre of the shocked region within a spot size of diameter 500 µm, so as to probe the region which experiences the most spatially uniform shock-wave profile. The energy of the pump beam is varied between 100 mJ (Intensity = 0.5 GW / cm^2) and 1320 mJ (Intensity = 6.5 GW / cm^2) in order to vary the peak pressure applied to the sample. The probe energy is kept fixed at 3 mJ throughout the experiment. The probe beam undergoes elastic (Rayleigh) and well as

inelastic (Stoke's and Anti-Stoke's) scattering from the compressed and uncompressed regions of the sample. The Rayleigh signal is filtered out by an ultra-steep notch filter and the scattered Raman signal is dispersed by a half-meter-long spectrometer (ANDOR Shamrock SR500i) followed by collection with a gated intensified CCD camera (ANDOR New iStar DH340) which has 2048 x 512 pixels.

For the experiment, a 1200 gr/mm grating is used, which enables us to record Raman spectra within the wave number range from 150 cm^{-1} to 1000 cm^{-1} with a spectral resolution of about 3 cm^{-1}. The target assembly is mounted on a motorized X-Y-Z-stage so that each shot can be taken on a fresh sample region. The gating time of the ICCD camera is kept at 2 ns. To achieve an acceptable signal to noise ratio, each Raman signal comprises 40 shots. So, overall, each Raman signal has a collection time of 80 ns. A greater number of shots could not be taken due to the associated increase in operating costs. During each shot, two quartz windows are damaged. However, signals from 40 shots are enough to extract reliable results.

Simulations:

1-D radiation hydrodynamics simulations are performed to model the experiment using the HYADES code [35]. HYADES is a Lagrangian radiation-hydrodynamics simulation code, which uses a flux-limited diffusion model of electron transport; in these simulations, the flux limit is set at 5% of the free-streaming limit. A multi-group diffusion approximation is employed to mimic thermal radiation transport within the target, utilizing 40 radiation groups arranged logarithmically from 1 eV to 2 keV. The equation of state (EOS) for glass and aluminium is taken from the SESAME library, while the EOS for Hexafluorobenzene is taken from an in-line Quotidian Equation of State (QEOS) model. This QEOS model takes as an input bulk modulus data from references 36 and 37.

Results and Analysis:

Hexafluorobenzene (purity 99.9 %) was obtained from Sigma-Aldrich and used for the experiments without any further purification. At ambient pressure, the Raman spectrum of Hexafluorobenzene was recorded which showed three prominent modes: C-F in-plan bending mode at 370 cm^{-1} (e_{1g} fundamental mode or ν_{10}), C-F out-of-plane bending mode at 445 cm^{-1} (e_{2g} fundamental mode or ν_6) and ring breathing mode at 560 cm^{-1} (a_{1g} fundamental mode or ν_1) which matches very well with the available reference [38], thereby providing some

reassurance regarding the purity of the sample. The Raman spectrum, obtained after the shock wave has entered into the sample, has contributions from both the shocked and unshocked regions. So, for analysis, we fit two or three Lorentzian peaks to the recorded curve out of which the first peak corresponds to the contribution from the unshocked region and the rest of the peaks correspond to contributions from the shocked region (depending on phase transitions occurring at high pressures). In the peak fitting process, we fix the position and FWHM of the first Lorentzian peak to that of the unshocked Raman curve while leaving the others free for best fitting. Thereby, we can separate the contributions of the unshocked and shocked regions in the resultant Raman spectra.

The pump beam was focussed at the glass-aluminium interface which leads to the generation of backward expanding plasma at the interface and drives a shock wave into the aluminium and thereafter into the sample. For the confined geometry employed here, the pressure in the aluminium foil is calculated using Fabbro's model [39] and is given by

$$P = 0.01\sqrt{Z}\sqrt{I}\sqrt{\frac{\alpha}{2\alpha+3}} \qquad \ldots(1)$$

Where P (in GPa) is the peak pressure in the aluminium, Z (in g/cm^2/s) is the reduced shock impedance, I (in GW/cm^2) is the laser intensity and α is a corrective factor to account for the confined geometry. The value of α is 0.1-0.4 for glass confinement [40]. Transfer of pressure from aluminium to Hexafluorobenzene was calculated using the impedance mismatch technique which requires knowledge of the Hugoniot of both of the materials. The Hugoniot is the locus of points in PV space that may be reached by the passage of a single shock wave from a given initial state (here approximately STP). The impedance mismatch technique relies upon the fact that as the shock wave passes the boundary between the two materials (of different impedance $Z = \rho_0.u_s$, where, ρ_0 is ambient condition density of the medium and u_s is the shock velocity in the medium) the pressure and particle velocity must equalise at the boundary. This enables the thermodynamic states of both materials to be established at the boundary based on a relatively limited set of measurements. Suppose, Z_A and Z_B are the impedance of the material A and B. If $Z_A > Z_B$, then the shock pressure transmitted in the sample B as well as reflected shock pressure in sample A will be lower then the shock pressure of the forward moving shock wave and vice-versa. In our experiment both the cases are taking place. Aluminium impedance is higher than Hexafluorobenzene resulting lower pressure in Hexafluorobenzene. Glass impedance is higher than Hexafluorobenzene resulting higher pressure jump in glass. The Hugoniot for aluminium was taken as U_s = 5.165 +

$1.25U_p$ (obtained from the SESAME library) while for Hexafluorobenzene, the Hugoniot was found using the QEOS model which forms a part of the HYADES code suite. This QEOS model takes as an input bulk modulus data from references 36 and 37. The Hugoniot so generated is given by $U_s = (2.736 \pm 0.056) + (1.278 \pm 0.002)\ U_p$.

Raman studies with varying pressure

All the three modes (ν_{10}, $\nu_{6,}$ and ν_1) were studied extensively with varying dynamic pressure in the range of 0.3 GPa (100 mJ) to 4.5 GPa (1320 mJ) at a fixed optical delay of 52 ns. All the three modes exhibit broadening as well as blue shift with an increase in dynamic pressure (similar to the results recorded with static compression) as shown in figure 2. Of the three modes, the symmetric stretching mode ν_1 (560 cm^{-1}) is the most intense and shows the largest shift with pressure. However, ν_{10} mode is also of equal interest, because it exhibits multiple (two) shocked peaks, apart from the unshocked one, thereby indicating the presence of a phase transition. Since laser-induced shock compression is a very sudden and short-lasting phenomenon; under shock compression with sufficient pressure, it can be concluded that Hexafluorobenzene directly goes from the liquid phase to solid phase-II [18] rather in solid phase-I. In the solid phase –I in decompression it does not come back to its initial state however, from solid phase-II, it comes back to initial state on decompression. In the static compression (slow compression), the phase transition is liquid phase to solid phase-I and in dynamic compression (fast compression), it is liquid phase to solid phase-II. In the solid phase the crystal structure is $P2_1/n(C_{2h}^5)$ with 6 molecule / unit cell [30]. This was verified with the time-resolved measurements discussed in the next section. It is observed that once the shock wave has completely crossed the sample, all of the Raman modes slowly return to their normal unshocked condition which demonstrates that this transition is of the second type.

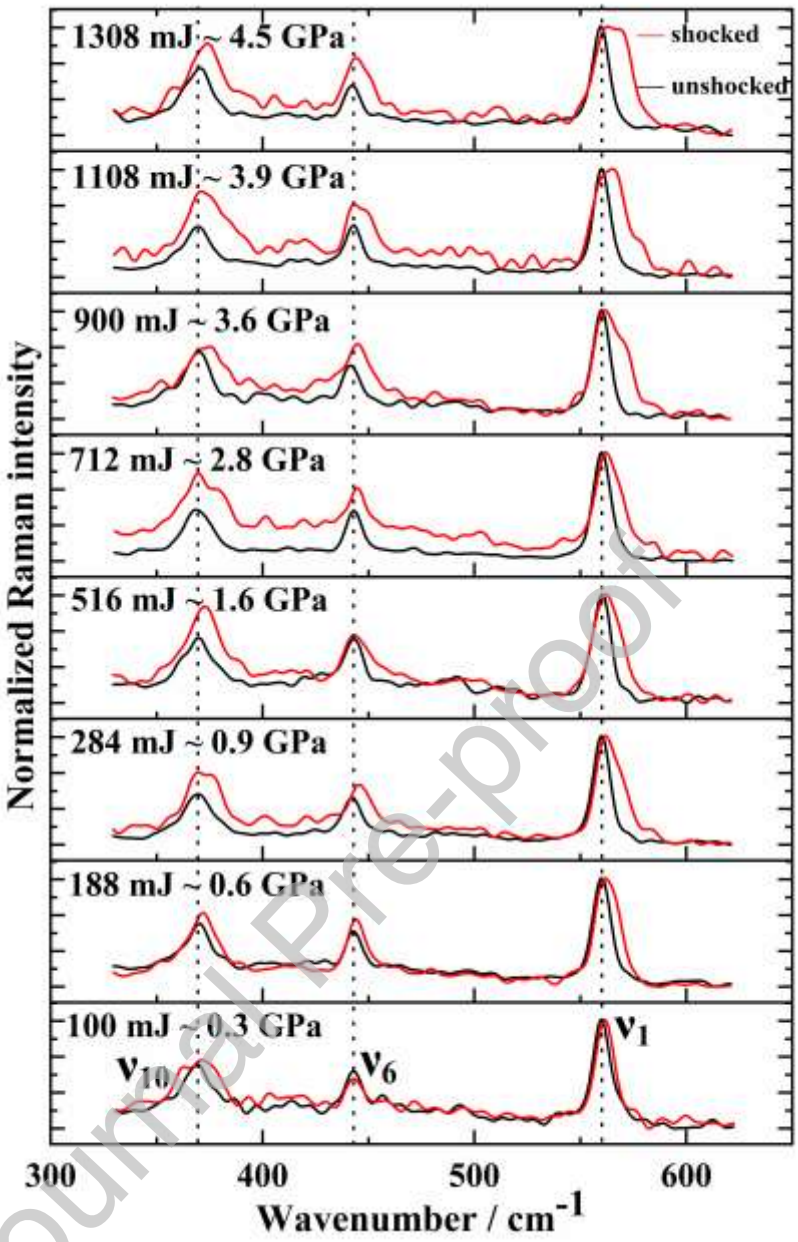

Fig. 2. Stacked Raman spectra of Hexafluorobenzene at various dynamic pressures: ranging from 0.3 GPa to 4.5 GPa. Black and red coloured spectra are from unshocked and shocked conditions respectively.

At a dynamic pressure of 0.9 GPa, the shocked peak of the ν_{10} mode starts to split marking the onset of the phase transition while at 2.8 GPa, the splitting can be clearly observed confirming the phase transition (liquid → Phase-II) as shown in figure 3a. On further application of pressure, this trend continues and the separation between the two split peaks continues to increase. So, under shock compression, the liquid → Phase-II phase transition starts at 0.9 GPa and the complete phase transition occurs at 2.8 GPa which is close to the static compression (0.8 GPa) data. On further increase of the shock pressure up to 4.5

GPa, the sample remains in the phase –II. Simulation results, at various laser energies, for a fixed delay of 52 ns have also been shown in figure 3b side-by-side for comparative study.

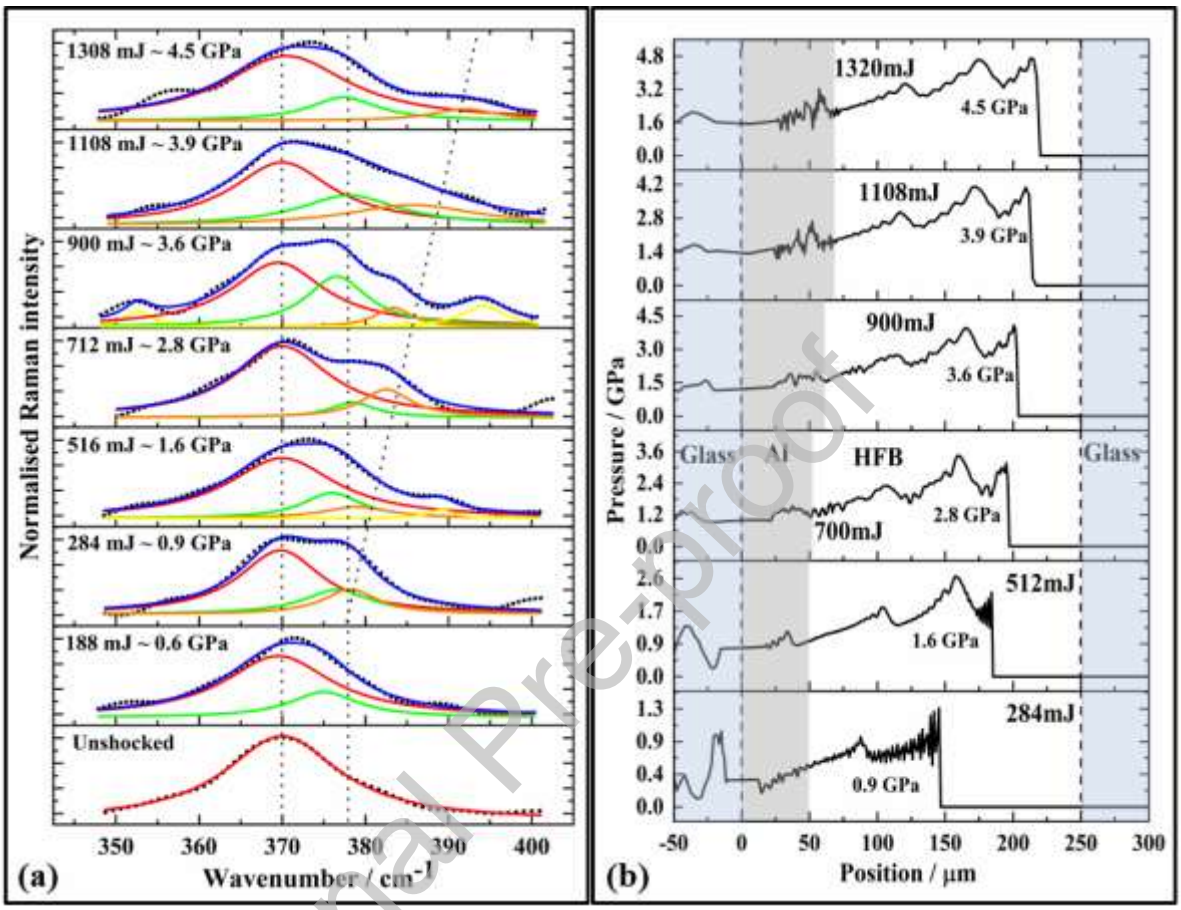

Fig 3a. The Lorentzian fit of shocked ν_{10} mode at different pressures; **b.** Pressure profile at different laser energies at a delay of 52 ns relative to the start of the pump pulse.

The other two modes were also studied in detail and the maximum blue shifts obtained in ν_6 mode and ν_1 mode were 7 cm^{-1} and 12 cm^{-1} respectively (at 4.5 GPa) thereby exhibiting a blue-shift rate of 1.55 cm^{-1} / GPa and 2.67cm^{-1} / GPa (on average) respectively. Under laser-driven shock compression, the observed shifts/ pressure are relatively less in comparison to data available in studies under static compression [30]. Variation of Raman shift for all three modes under shock compression and static compression has been shown in figure 4. Experiments were repeated multiple times to eliminate any experimental errors or uncertainties that might have crept in the first time due to the complexity of these experiments and the results obtained were similar every time. Hence, it can be confidently stated that in the case of Hexafluorobenzene, laser-driven shock compression yields relatively

less blue shifts in all the three studied Raman active modes in comparison to static compression. This is due to the fact that the laser-driven shock compression is a Hugoniot associated with the high temperatures, whereas static compression is isothermal.

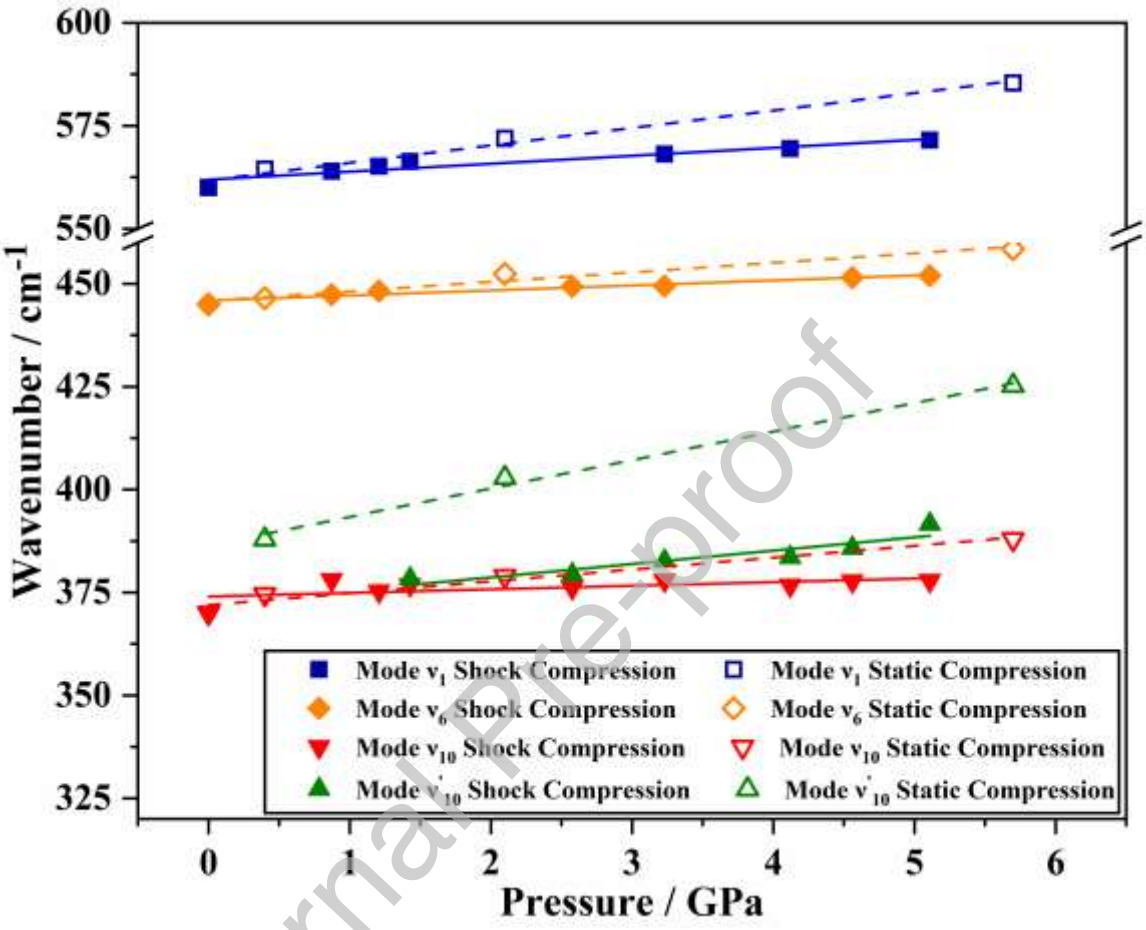

Fig. 4. Comparison of Raman shift obtained under shock and static compression (Solid lines are a linear fit to the shock compression data; dotted lines are a linear fit to the static compression data from ref [30]) in ν_1, ν_6, and ν_{10} modes.

Gruneisen parameter calculations

A Gruneisen parameter is a non-dimensional quantity that describes the effect of pressure or change in volume on the vibrational properties of materials. It has been shown that mode Gruneisen parameters are inter-related with bond anharmonicity [29]. The mode Gruneisen parameter γ_i, for the i^{th} vibrational mode of a crystal with frequency ν_i, is given by

$$\gamma_i = -\frac{d(\ln \nu_i)}{d(\ln V)} \quad \ldots(2)$$

On integrating this equation, we get

$$\frac{\nu_i(P)}{\nu_i(0)} = \left\{\frac{V(0)}{V(P)}\right\}^{\gamma_i} \quad \ldots(3)$$

Taking the natural log on both sides, we get

$$ln\left\{\frac{\nu_i(P)}{\nu_i(0)}\right\} = \gamma_i\, ln\left\{\frac{V(0)}{V(P)}\right\} = \gamma_i\, ln\left\{\frac{\rho(P)}{\rho(0)}\right\} \quad \ldots (4)$$

Where γ_i is mode Gruneisen parameter, *V(0)* and *V(P)* are the volumes of bulk solid at atmospheric pressure and at an applied pressure *P*. $\nu_i(0)$ and $\nu_i(P)$ are the vibrational wave number at atmospheric and applied pressure *P*. Clearly, the slope of the log-log plot of relative frequency shift *versus* relative volume change (or relative density change) for a vibrational mode gives us the Gruneisen parameter for that mode. For all the three Raman active modes that we studied, $\nu_i(P)$ was obtained experimentally while the relative density ratio was obtained from simulations. Relative frequency change *vs.* relative density change under shock compression for the three modes has been shown in figure 5. The values of the slopes i.e., the Gruneisen parameters corresponding to the ν_{10}, ν_6, and ν_1 modes are 0.0095 ±0.0140, 0.0433 ± 0.0060, and 0.0561 ± 0.0044 respectively.

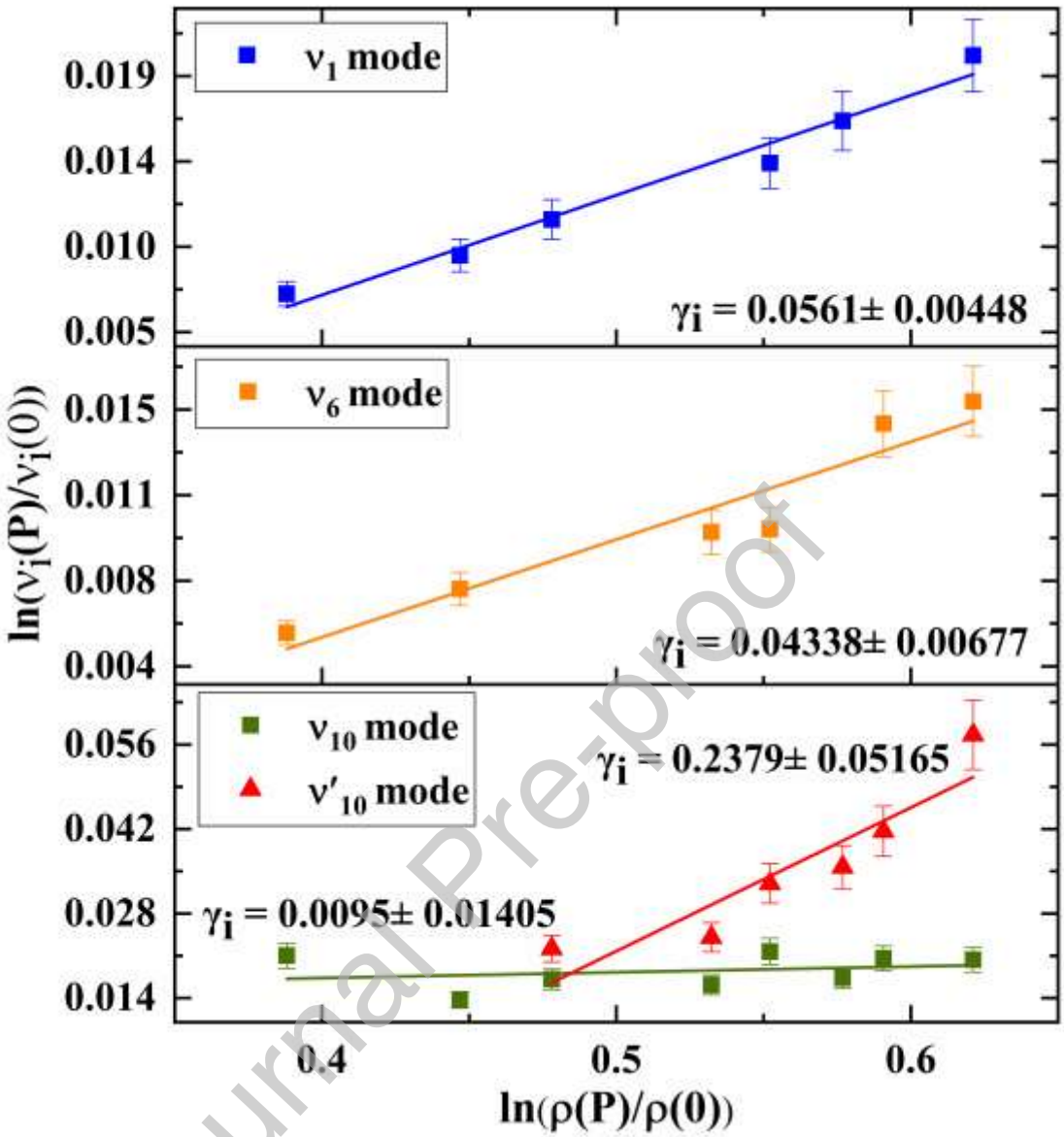

Fig. 5. Log-log plot of relative frequency change *vs.* relative density change under shock compression for the three modes (ν_{10}, $\nu_{6,}$ and ν_1).

Raman studies with increasing time delay and determination of shock velocities

To understand the propagation of shock waves into the sample, we have analysed time-resolved data for all modes, however, for the sake of brevity of the manuscript, detailed time delay analysis of only ν_1 mode at two different laser energies, 300 mJ (~1.43 GPa) and 500 mJ (~2.58 GPa), is presented here, as shown in Figures 6 and 7 respectively. The time delay between pump and probe is varied from 10 ns to 101 ns. Experimental results are presented in

figure 6a and 7a whereas simulation results are shown in figure 6b and 7b for comparative studies.

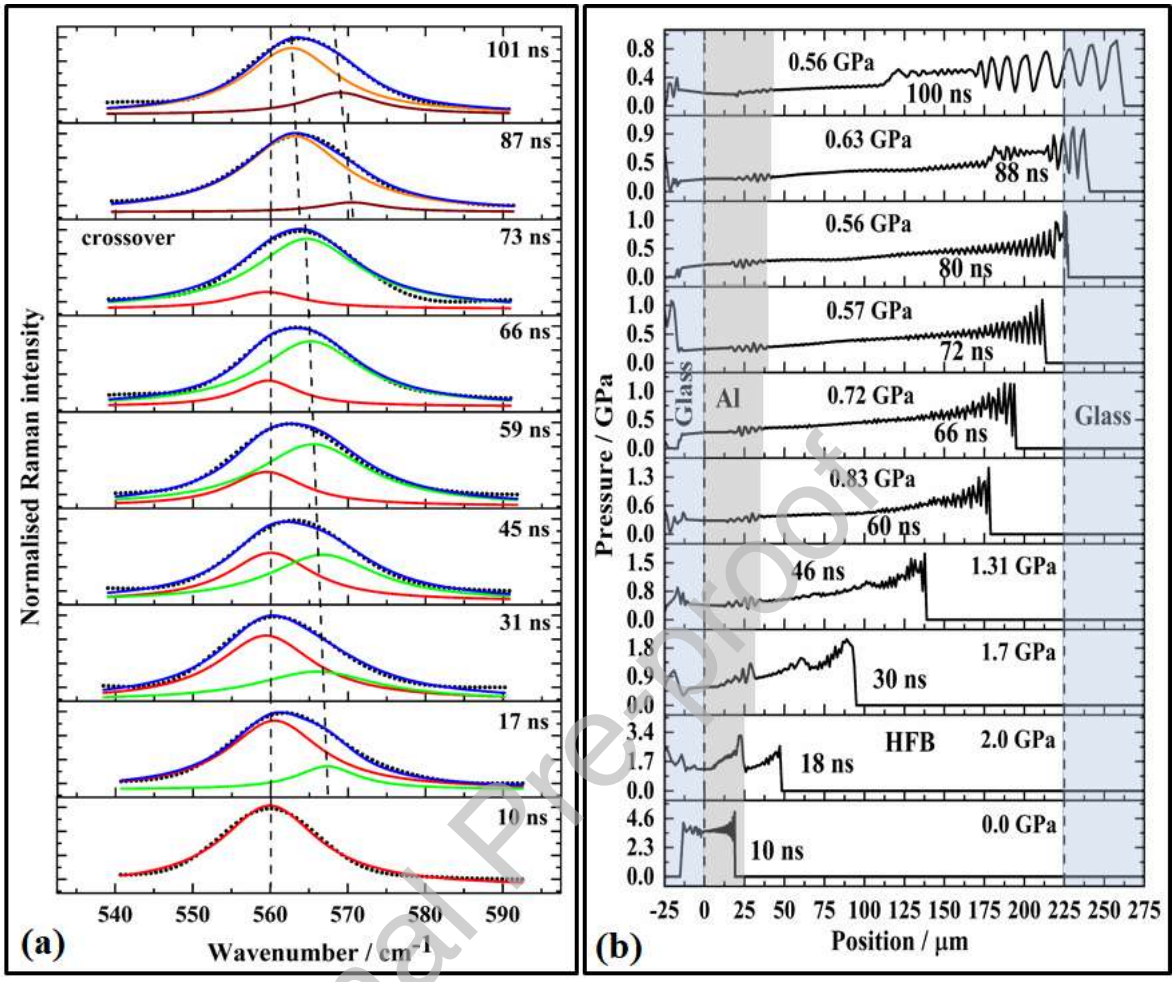

Fig 6a. Lorentzian fit of shocked ν_1 (560 cm^{-1}) mode for different delay times; **b.** The spatial profile of shock waves at different delay times for laser energy of 300 mJ was obtained from 1-D radiation-hydrodynamics simulations.

The red and green curves represent contributions from unshocked and shocked regions respectively while the blue curve is the cumulative peak of the two. The dotted curve represents the experimental data. At a delay of 10 ns, it can be seen that there is no broadening observed in the Raman mode. This means the shock wave has not entered in the C_6F_6 yet and the same can be seen from the simulation results that the shock wave is still in aluminium. At 17 ns, a small green peak at a higher frequency indicates that the shock wave has entered into the sample and travelled a very small distance. The same can be seen from the simulation result at the same delay (18 ns). As the delay is increased, the shock wave travels deeper into the sample, and hence more regions of the sample experience high

pressure. Since the experimental spectra are made up of contributions from both shocked and unshocked regions, the contribution of the shocked region increases with delay due to the fact that the shock has propagated further into the sample. So, we see the area under the green peak increasing as the delay is increased. Here, we also observe that the shocked Raman peak is shifting slightly towards the lower frequency side with increasing delay, which would not be the case if the shock wave retained its original strength as it traversed the medium. To better understand our results, we carefully analysed the simulation output. In the simulation results as well, it was observed that, as time progresses, the shock wave amplitude reduces. This reduction in peak pressure is expected given that the laser is no longer driving the shock at these late times, so it is expected to decay in strength as it propagates. Hence, although, the area under the green (shocked) peak increases with delay, overall, we see a slight redshift in the green peak. Between 73 ns and 87 ns delay, the shock wave reaches the far end of the sample and gets reflected from the interface with slightly higher pressure (because of the higher impedance of glass compared to C_6F_6). It can also be seen from the simulation results that at 80 ns, the shock wave has completely traversed the length of the sample, and on increasing the delay even further it gets reflected from the interface at a higher pressure. However, the reflected shock wave is quickly decaying because it catches up with the rarefaction wave of the incident shock wave as well. So, at 87 ns, we see a brown peak appearing at a higher wavenumber because of the reflected shock wave along with an orange peak which corresponds to the material which has only been traversed by the forward going shock. As the delay is increased to 101 ns, both of the peaks show a redshift because of a decrease in pressure, and the overall area covered by the brown peak has increased because the reflected shock wave has travelled deeper into the sample. Similarly, Fig. 7a and Fig. 7b show experimental time-resolved measurements and simulation results respectively for a laser energy of 500 mJ. The different colour peaks have the same meaning as explained earlier. From experimental results, it appears that with a laser energy of 500 mJ, the shock wave crossover time is somewhere between 59 ns and 66 ns. This is concluded by considering the fact that at a delay of 59 ns no other extra peak is observed at a higher frequency, however, at a delay of 66 ns, one small peak emerges at the higher frequency side indicating that the shock wave has already been reflected from the sample-glass interface with higher pressure (again, because of impedance mismatch). The exact time at which the shock wave reaches to interface could not be measured as in our case the minimum time delay step is 7 ns restricted by the round-trip time of the probe beam between the two parallel mirrors used for generating the delay. In the simulation, time steps of 2.5 ns have been taken

and it can be seen that the shock wave reached the interface at 62 ns which matches very well with the experimental observation. Afterward, the reflected shock wave increases the pressure even further which results in the appearance of a new brown peak at a higher wavenumber along with an orange peak due to the previously shocked region. On increasing the time delay even further, both of these peaks exhibit redshift, as explained earlier.

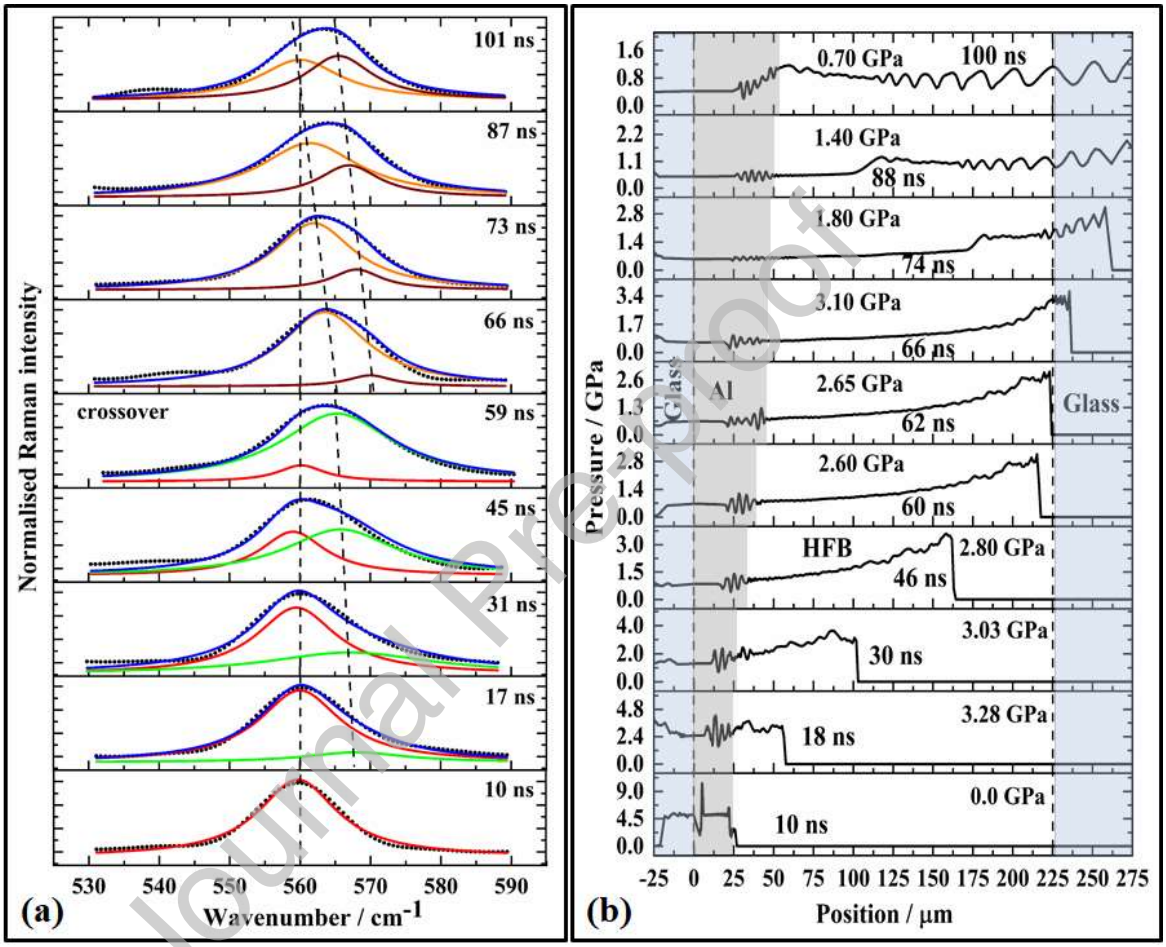

Fig 7a. Lorentzian fit of shocked v_1 (560 cm^{-1}) mode for different delay times, **b.** The spatial profile of the shock waves at different delay times for laser energy of 500 mJ was obtained from one-dimensional radiation-hydrodynamics simulations.

The shock velocity is experimentally calculated by using the equation $U_s = r.x$ where x is the sample thickness (200 μm) and r is the slope of the intensity ratio $I_{shocked}/(I_{shocked} + I_{unshocked})$ *Vs* time delay plot as shown in figure 8. These intensity ratios are obtained from the curve fitting of the experimental data (See Figures 6a & 7a). To

verify, shock velocities are also calculated using simulation data by plotting the fraction of the volume of the sample traversed by the shock wave as a function of a time delay. This is also presented in figure 8 along with the experimental data. At laser energies of 300 mJ and 500 mJ, the values of *'r'* come out to be 0.01272 and 0.01825 and the corresponding shock velocities are 2.54 km/s and 3.65 km/s respectively which are in close agreement with the simulation results of 2.98 km/s and 3.84 km/s respectively at the same laser energies.

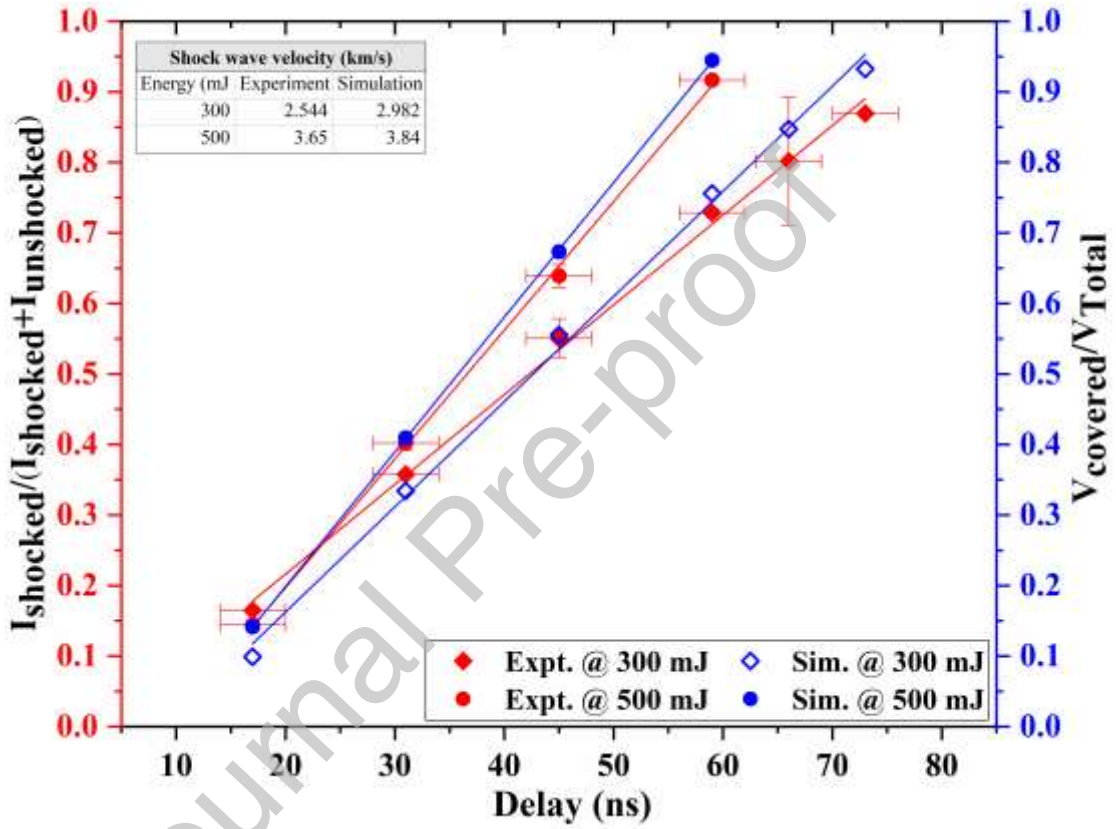

Fig. 8. The slope of the graph from the experimental and simulations data represent the shock wave velocities at laser energies of 300 mJ and 500 mJ respectively.

Conclusion:

In this study, we have presented the findings of Raman studies on Hexafluorobenzene when subjected to laser shock compression up to 4.5 GPa. In total, three Raman active modes were investigated: 370 cm^{-1} (ν_{10} mode), 445 cm^{-1} (ν_6 mode) and 560 cm^{-1} (ν_1 mode) in the dynamic pressure range of 0.3 GPa to 4.5 GPa. Of the three modes, the symmetric stretching mode ν_1 is the most intense one and shows a blue shift of about 2.67 cm^{-1} / GPa while the ν_6 mode

shows the least blue shift out of the three. A signature of the liquid → Phase-II phase transition was observed at about 0.9 GPa and completed by 2.8 GPa. The shock velocities deduced from the experimental data using Time-resolved measurements for the laser energies: 300 mJ (1.43 GPa) and 500 mJ (2.58 GPa) are 2.54 km / s and 3.65 km / s respectively which are in close agreement with shock velocities obtained from 1-D radiation-hydrodynamics simulations for the same laser energies which are 298 km /s and 3.84 km /s respectively. The Gruneisen parameters corresponding to the $\nu_{10,}$ ν_6, and ν_1 modes are calculated as 0.00950 ±0.0140, 0.0433 ± 0.0060, and 0.0561 ± 0.0044 respectively

Conflict of Interest

We confirm that this manuscript has not been published and is not under consideration for publication elsewhere. We have no conflicts of interest to disclose.

References:

[1] Drake R P, "High-Energy-Density Physics". Springer, 2006.

[2] Duffy T S, Smith R F, "Ultra-High Pressure Dynamic Compression of Geological Materials". Front. Earth Sci. 2019. 7:23

[3] Hurricane O A, Callahan D A, Casey D T, Celliers P M, Cerjan C, Dewald E L, Dittrich T R, Döppner T, Hinkel D E, Berzak Hopkins L F, Kline J L, Le Pape S, Ma T, MacPhee A G, Milovich J L, Pak A, Park H S, Patel P K, Remington B A, Salmonson J D, Springer P T, Tommasini R, "Fuel gain exceeding unity in an Inertially confined fusion implosion". Nature. 2014. 506(7488): 343–348.

[4] Rice M H, McQueen R G, Walsh J M, "Compression of Solids by Strong Shock Waves". Solid State Physics. 1958. 1–63.

[5] Gupta Y M, Pangilinan G I, Winey J M, Constantinou C P, "Time-resolved molecular changes in a chemically reacting shocked energetic liquid". Chem. Phys. Lett. 1995. 232: 341-345.

[6] Hare D E, Franken J, Dlott D D, "A new method for studying picoseconds dynamics of shocked solids: application to crystalline energetic materials". Chem. Phys. Lett. 1995. 244(3): 224-230.

[7] Pangilinan G I, Gupta Y M, “Use of time-resolved Raman scattering to determine temperatures in shocked carbon tetrachloride”. J. Appl. Phys. 1997. 81(10): 6662-6669.

[8] Helminiak, Nathaniel Steven, "Construction and Characterization of a Single-Stage Dual Diaphragm Gas Gun" (2017). Master's Theses (2009-). 441. http://epublications.marquette.edu/theses_open/441.

[9] Trunin R F, “Shock compressibility of condensed materials in strong shock waves generated by underground nuclear explosions”, UFN, 164:11 (1994), 1215–1237; Phys. Usp., 37:11 (1994), 1123–1145S.

[10] Luo S N, Swift D C, Tierney T E, Paisley D L, Kyrala G A, Johnson R P, Hauer A A, Tschauner O, Asimow P D, “Laser-induced shock waves in condensed matter: some techniques and applications”. High Press. Res. 2004. 24(4): 409-422.

[11] Banishev A A, Shaw W L, Dlott D D, “Dynamics of polymer response to nanosecond shock compression” Appl. Phys. Lett. 2014. 104(10): 101914-4.

[12] Kobayashi T, Sekine T, “In Situ Raman spectroscopy of shock-compressed benzene and its derivatives”, Phys. Rev. B. 2000. 62(9):5281-5284.

[13] Hiyama T, “Organofluorine compounds, Chemistry, and Applications”. Springer, 2000.

[14] Kirsch P, “Modern fluoro-organic chemistry, synthesis, Reactivity, Applications”. Wiley-VCH: Weinheim, Germany, 2004.

[15] An B K, Gihm S H, Chung J W, Park C R, Kwon S-K, Park S Y, “Color-Turned Highly Fluorescent Organic Nanowires/ Nano fabrics: Easy Massive Fabrication and Molecular Structural Origin”. J. Am. Chem. Soc. 2009. 131(11): 3950-3957.

[16] Berger R, Resnati G, Metrangolo P, Weber E, Hulliger J, “Organic Fluorine Compounds: a great opportunity for enhanced materials properties”. Chem. Sov. Rev. 2011. 40(7): 3496-3508.

[17] Neel A J, Milo A, Sigman M S, Toste F D, “Enantodivergent Fluorination of Allylic Alcohols: Data set design reveals Structural interplay between achiral directing group and achiral anion”. J. Am. Chem. Soc. 2016. 138(11): 3863-3875.

[18] Suzuki Y, Shimada H, Shimada R, "High-pressure Raman Study of Hexafluorobenzene Crystals". Bull. Chem. Soc. Jpn. 1996. 69(11): 3081-3088.

[19] Raja G, Saravanan K, Sivakumar S, "Analysis on vibrational spectra of Hexafluorobenzene based on density functional theory calculations". Elixir Comp. Chem. 2011. 32(2011): 2111-2115.

[20] Mason R P, Rodbumrung W, Antich P P, "Hexafluorobenzene: a sensitive 19F NMR indicator of tumor oxygenation". NMR Biomed. 1996. 9(3): 125–134.

[21] Zhao D, Constantinescu A, Chang C H, Eric Hahn W, Mason Ralph P, "Correlation of Tumor Oxygen Dynamics with Radiation Response of the Dunning Prostate R3327-HI Tumor". Radiat Res. 2003. 159 (5): 621–631.

[22] Patrick C R, Prosser G S, "A Molecular Complex of Benzene and Hexafluorobenzene". Nature. 1960. 187(4742): 1021.

[23] Boden N, Davis P P, Stam C H, Wesselink G A, "Solid Hexafluorobenzene". Mol. Phys. 1973. 25(1): 81-86.

[24] Budzianowski A, Katrusiak A, "Pressure-frozen benzene I revisited". Acta Cryst. 2006. B62: 94-101.

[25] Rusek M, Kwasna K, Budzianowski A, Katrusiak A, "Fluorine…Fluorine Interactions in a High-Pressure Layered Phase of Perfluorobenzene". J. Phys. Chem. C. 2020. 124(1): 99-106.

[26] Caibini L, Gorelli F A, Santoro M, Bini Roberto, Schettino Vincenzo, Mohamed Mezouar, "High-pressure and high-temperature equation of state and phase diagram of solid benzene". Phys. Rev. B. 2005. 72(9): 094108-1-094108-7.

[27] Katrusiak A, Podsiadlo M, Budzianowski A, "Association CH… π and No van der Waals Contacts at the Lowest Limits of Crystalline Benzene I and II Stability Regions". Cryst. Growth Des. 2010. 10(8): 3461-3465.

[28] Wen X D, Hoffmann R, Ashcroft N W, "Benzene under High Pressure: a Story of Molecular Crystals Transforming to Saturated Networks, with a Possible Intermediate Metallic Phase". J. Am. Chem. Soc. 2011. 133(23): 9023-9035.

[29] Cansell F, Fabre D, Petitet J P, “Chemical transformations of benzene under high pressure and at high temperature”. High-Pressure Research, 1991. 7:1-6, 127-129

[30] Pravica M, Sneed D, Wang Y, Smith Q, White M. “Hexafluorobenzene under Extreme Conditions”. J. Phys. Chem. B. 2016. 120(10): 2854-2858.

[31] Wang Y, Wang L, Zheng H, Kuo Li, Michał Andrzejewski, Takanori Hattori, Asami Sano-Furukawa, Andrzej Katrusiak, Yu-Fei Meng, Fuhui Liao, Fang Hong, Ho-kwang Mao “Phase Transitions and Polymerization of C_6H_6–C_6F_6 Cocrystal under Extreme Conditions”. J. Phys. Chem. C. 2016. 120(51): 29510-29519.

[32] Remo J L, Hammerling P X, "Experimental and computational results for 1054-nm laser-induced shock effects in confined meteorite and metallic targets". In High-Power Laser Ablation III, Claude R. Phipps, Editor, Proceedings of SPIE 2000, 4065: 635.

[33] Chaurasia S, Rastogi V, Rao U, Deo M N “Development of in situ time-resolved Raman Spectroscopy facility for dynamic shock loading in materials”. Journal of Instrumentation. 2017. 12: P11008.

[34] Rastogi V, Rao U, Chaurasia S, Sijoy C D, Mishra V, Deo M N, “Time-Resolved Raman spectroscopy of Polytetrafluoroethylene under laser shock compression”. Appl. Spec. 2017. 71(12): 2643-2652.

[35] HYADES is a commercial product of Cascade Applied Sciences email: larsen@casinc.com

[36] Dymond J H, Glen N, Robertson J, and Isdale J S, “(p, ρ, T) for $\{(1-x)C_6H_6+xC_6D_6\}$ and $\{(1-x)C_6H_6+xC_6F_6\}$ in the range 298 to 373 K and 0.1 to 400 MPa”, J. Chem. Thermodynamics, 1982, 14: 1149-1158.

[37] Dymond J H, Robertson J, and Isdale J S, “Transport Properties of Nonelectrolyte Liquid Mixtures – IV. Viscosity Coefficients form Benzene, Perdeuterobenzene, Hexafluorobensine, and an Equimolar Mixture of Benzene + Hexafluorobenzen from 25 to 100 °C at Pressures up to the Freezing Pressure, International Journal of Thermophysics, 1981, 2(3): 223-236.

[38] Raman spectra of Hexafluorobenzene. Retrieved from https://www.chemicalbook.com/SpectrumEN_392-56-3_Raman.htm

[39] Fabbro R, Fournier J, Ballard P, Devaux D, Virmont J, “Physical study of laser-produced plasma in confined geometry”. J. Appl. Phys. 1990. 68(2): 775-784.

[40] yu H, Wu X, Yuan Y, Lee H, Yang J, “Confined geometry and laser energy affect laser plasma propulsion”. Optics Express. 2019. 27(7): 9763-9772.